

PA3900 Research Project

Observing Transiting Exoplanets

Measuring the decrease in flux observed from a star as an exoplanet transits in front of it can be used to derive fundamental physical parameters of the exoplanet and its parent system. This project describes the use of the Oadby Observatory to measure the photometric light curve of the transit of two confirmed exoplanets and one unpublished candidate exoplanet. Using the transit depth in conjunction with stellar parameters from TESS[1] and Gaia[2], we used AstroImageJ[3] to determine the radius of each confirmed and candidate exoplanet. The first exoplanet, HAT-P 61 b ($P=1.9$ days, $R_* = 0.938 \pm 0.011 R_\odot$ [4]), measured a transit depth of 0.86%, resulting in a radius of $0.87 \pm 0.04 R_J$. The second, and largest exoplanet observed, XO-3 b ($P=0.938$ days, $R_* = 1.54 \pm 0.11 R_\odot$ [5]), exhibited a transit depth of 1.08%, resulting in a radius of $1.48 \pm 0.1 R_J$. The final transit observed was of the unpublished candidate exoplanet TOI-3887 ($P=4.24424$ days[1], $R_* = 1.57 R_\odot$ [2]). The transit measured for this candidate exoplanet was 0.99% which led to a radius of $1.39 R_J$. From orbital and planetary characteristics it was concluded that all three of these exoplanets are hot Jupiters experiencing large amounts of stellar radiation. Radii measurements for HAT-P 61 b and XO-3 b fell within one uncertainty bar of chosen literary values, however, it is important to consider different measurements are concluded by a variety of literature on each exoplanet. This is not the case for TOI-3887 as there are no published results on the physical characteristics of the exoplanet.

1 Introduction

A main focus of modern astronomy has been finding and observing exoplanets, planets outside of our solar system. Since the discovery of the first exoplanet in 1992 [6], thousands of 'super-Earths,' 'mini-Neptunes,' and 'hot Jupiters' have been since confirmed through missions like Kepler, K2 and the Transiting Exoplanet Survey Satellite (TESS). One of the most effective methods of detecting these exoplanets is the transit method, which measures the amount of light seen from a star as one, or several, of its planets cross in front of it. This method creates a distinctive light curve that can be used to determine physical details about the planet such as its radius, atmospheric composition, and orbital period, as well as details about its parent system such as the presence of other exoplanets or moons. The transit method uses observation techniques to measure the amount of light detected by a star as a planet crosses in front of it along the observer's line of sight. As the planet crosses, it blocks out a small

amount of light, creating a dip in the light curve, the depth of this dip is proportional to the square of the ratio of the planet's radius (R_P) to the star's radius (R_*), providing direct insight to the planets radius if the radius of the star is known. Observing transits has become more powerful with the advancements in telescope technology, providing the ability to detect smaller, even Earth-sized planets. However, the transit method is not without limitations. When determining the host star radius, uncertainties in luminosity, effective temperature, and spectral type will all directly affect the reliability of determined R_P values. Furthermore, limb-darkening, the optical effect in which the centre of a star's disk appears brighter than the edge, complicates light curve analysis, necessitating wavelength-dependent corrections to avoid systematic errors.

This paper will discuss the advantages and limitations of using the transit method to calculate exoplanet radii. Exploring theoretical foundations, experimental processes, and analytical techniques involved when studying transit-

ing exoplanets. Although we will discuss how light curves can be used to determine atmospheric compositions and orbital periods, the focus of this paper will be to use data gathered to find the radii of exoplanets whose transits we have observed.

2 Theory

2.1 FUNDAMENTALS OF THE TRANSIT

In order for a transiting exoplanet to be seen from an observer on Earth, a transit of orbital inclination near 90° is required. The orbital inclination is the angle at which the planet's orbit is tilted about the observer, 90° orbital inclination can also be described as having an impact parameter, b , equal to zero.

When a transit has sufficient impact parameter to be observed from Earth, it will be seen to have four stages, as shown in Figure 1. Stage one (ingress) begins as soon as the planet starts to pass in front of the star, with Stage two beginning when the disk of the planet is completely in front of the star from the perspective of the observer. Stage three begins the reverse of the previous two stages and is called the egress, and the transit is finalized at stage four in which the planet is no longer covering any part of the star's disk.

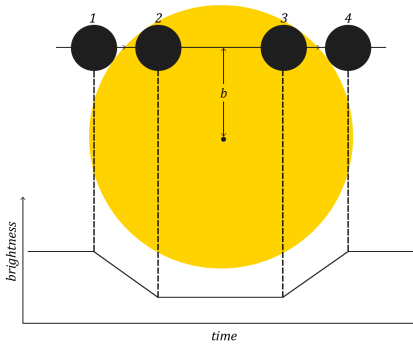


Figure 1: Stages of the Transit Process (Created by Student 229017963, 2025).

Given that not all planets orbiting stars outside our solar system will have an orbital inclination of 90° , and assuming that the distribution of orbital inclinations is random, there will be an associated transit probability for a given star system. This is an important variable as it can give rise to an expected number of transits for a number of observed systems. The transit probability can be found by looking at the transit geometry as shown in figure 2, where the impact parameter is given by $b = a \cos i$. A

transit will only be observable if b is less than the radius of the star, R_* , or more precisely, the combination of the radius of the star and the planet, $R_* + R_P$. Rearranging for $\cos i$ yields: $\cos i \leq \frac{R_* + R_P}{a}$. And because $\cos i$ is uniformly distributed between zero and one it can be directly replaced by the probability, giving rise to the transit probability equation:

$$P = \frac{R_* + R_P}{a} \quad (1)$$

This can be simplified to omit the radius of the planet as in most cases it is negligible when compared to the radius of the host star.

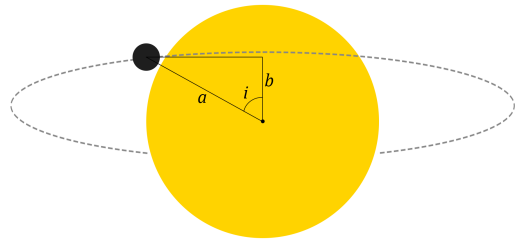


Figure 2: Transit Geometry (Created by Student 229017963, 2025).

Unfortunately, equation 1 cannot be used for all exoplanets as it assumes a circular orbit. For an orbit with eccentricity ($e > 0$), the derivation for transit probability is more complex and incorporates the shadow cast upon the star from the exoplanet from the observer's point of view. Resulting in higher transit probabilities in eccentric orbits than circular [7].

$$P = \frac{R_*}{a(1 - e^2)} \quad (2)$$

This increased transit probability suggests that the majority of discovered exoplanets would have eccentric orbits, an idea that is reinforced by the fact that the majority of discovered exoplanets do have eccentric orbits.

Another effect of eccentric orbits is that the orbiting planet will not have a constant angular momentum. Kepler's Second Law states that a planet must maintain angular momentum throughout its motion, or that a planet will sweep out equal area in equal time. Meaning that a planet in eccentric orbit must have higher than average velocity near perihelion (when closest to the star), and lower than average velocity at aphelion (when furthest from the star).

This principle directly affects transit times, the planet will exhibit a significantly shorter transit if observed at perihelion and a longer transit time at aphelion. Using the vis-viva equation, which models the velocity of an orbiting body, the velocities at perihelion and aphelion can be derived:

$$v_p = \sqrt{\frac{GM}{a} \frac{1+e}{1-e}} \quad (3)$$

$$v_a = \sqrt{\frac{GM}{a} \frac{1-e}{1+e}} \quad (4)$$

Photometric light curves measured are unfortunately never as simple as shown in Figure 1, and one phenomenon that adds complexity to light curves is called limb-darkening, and it is the effect that causes the edges, or limbs, of a stellar disk to have a lower specific intensity, $I_\lambda(\mu)$, than the centre. This appears partly due to the temperature gradient within the solar photosphere, in which the closer you get to the centre of the star, the hotter it becomes. And also partly due to the optical depth of photons escaping the star. A simple model for limb-darkening describes an analytical solution for an atmosphere in which the source function is linear in optical depth, and is given by[8]:

$$\frac{I_\lambda(\mu)}{I_\lambda(1)} = 1 - x_\lambda(1 - \mu) \quad (5)$$

Where $\mu = \cos \theta$, where θ is the angle between the normal and angle of viewing, and x_λ is the linear limb-darkening coefficient. Other models including the quadratic, three and four-parameter non-linear can be used and can return more realistic results however accounting for limb-darkening is outside the scope of this project, and the phenomenon is therefore only being explained to assist in analyzing the shape of the light curve obtained during observations.

Another effect that can make transit observations more difficult is stellar activity. Stars do not emit perfectly uniform light but can display sunspots, granulation and solar flares, all of which create brighter and darker areas of the stellar disk. If a transiting exoplanet travels across a region of varying brightness, the measured flux will deviate from the expected light curve. These variations can also lead to errors in limb-darkening models that have been fitted to the data, which expect a smooth decrease and increase in measured flux. A simulated example of the deviation of measured flux from transiting across a sunspot can be seen in figure 3.

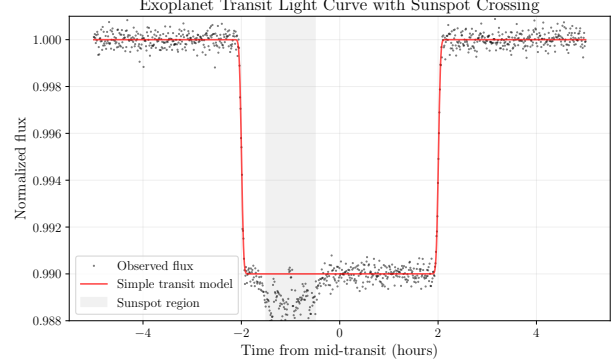


Figure 3: Example exoplanet light curve showing the effect of an exoplanet crossing a dark sunspot (Created by Student 229017963, 2025).

In addition to the primary transit, of which the exoplanet crosses in front of the star, there is a secondary transit, where the exoplanet passes behind the star, temporarily blocking any light that it may have been reflecting from the star. This secondary transit can provide insight into the exoplanet's temperature and reflectivity. By comparing the measured decrease in flux through the infrared and visible wavelengths, information about the heat reflectivity efficiency can be measured. Spectroscopy can also be used during the secondary transit by subtracting the star's spectrum to isolate the planet's spectrum, this method has been used to detect molecules like water vapour, carbon dioxide and methane, providing an insight into exoplanet atmospheres.

2.2 TRANSIT ANALYSIS

The main task of this project is to find the radius of a target exoplanet, one of the most useful planetary properties that can be obtained from a transit observation. To do this the transit depth must be found, the fractional decrease in observed flux when the planet passes in front of the star. Given by:

$$\Delta F = \frac{F_i - F_o}{F_i} \quad (6)$$

Where ΔF is the fractional change in flux, usually measured as a percentage, F_i is the flux of the unobstructed star and F_o is the flux of the star with the exoplanet completely in front of it. This can be used to derive the transit depth equation by relating the flux of the star to its surface area, $F_o \propto A_* - A_P = \pi R_*^2 - \pi R_P^2$. Substituting this into equation 6 yields the transit depth equation:

$$\Delta F = \left(\frac{R_P}{R_*} \right)^2 \quad (7)$$

This transit depth equation can be rearranged to find the radius of the exoplanet if the radius of the star is known.

Another property that can be observed is the height and composition of the exoplanet's atmosphere, as the exoplanet passes in front of its host star, light from the star will pass through the planet's atmosphere. As it does, specific molecules in the atmosphere will absorb certain wavelengths of light, leading to a transit spectrum, a spectrum that displays changes in the wavelength emitted making it possible to determine specific molecules in an exoplanet's atmosphere. This is not something that we will be pursuing in this project, however, it is important to discuss as it displays how useful the transit method can be for identifying planets and their properties.

In addition to transit depth and atmospheric composition, Transit Timing Variations (TTVs) can provide insight into more complex multi-planetary systems even if the planets cannot be observed directly or via a transit. Transit Timing Variations occur when an exoplanet orbit deviates from expected transit times based on basic orbital models, this is usually due to gravitational interactions with other planets in the system. Additional planets in the same system will induce gravitational forces upon each other, causing variational changes in the timing of transits. By analyzing these variations, it is possible to identify how many planets may be in the system that is being observed. This is especially effective with resonant planetary systems, where the orbital periods are related by simple ratios.

3 Experimental

3.1 TARGET SELECTION

A list of possible targets along with their transit times and dates had to be acquired in order to effectively plan dates and times as well as look ahead at weather conditions. This was done at the beginning of the project using NASA's Exoplanet Archive [9], a database of over 13,000 confirmed and candidate exoplanets with information on each one. However, given the Oadby Telescope's sensitivity, our position on Earth and the time of year we had to filter through the database to get realistic target candidates. Filters included; a transit depth greater than 0.8%; an apparent magnitude less than 14; a declination above 0°; and a right ascension between 45° and 210°. These filters left 30 exoplanets that would be observable from the Oadby Telescope in the date range that we would be observing.

With this list of planets, we then used the Transit Prediction Service [10] to see what the times and dates of each transit would be, along with airmass plots for each one. Adding all this into a data sheet we created a table

of all possible transits with their respective exoplanets for the date range we would be observing, see appendix A for the full candidate list table. Using this list we were able to check the weather in advance for a possible transit observation.

It should be noted that not all exoplanet transits observed are on the initial list just described, this is because clear nights were not common during our period of observation and when a night of favourable seeing conditions arose, we would expand our exoplanet list if there was not one already planned to transit that night. For example, our first chance of observation was on February 24, 2025, when the sky was only clear earlier in the night, with our list only having transits later in the night we chose an exoplanet with a transit depth slightly less than 0.8%, HAT-P 61 b. It was not on the list however it had an earlier transit so we chose to observe it given the circumstances.

This is the case for two of the three transits observed. Transits that were not initially on the list but were observed due to the expanded exoplanet search are highlighted on the transit candidate list.

3.2 OBSERVATIONAL SETUP

The telescope used is a PlaneWave CDK20 equipped with Movian Instruments' G3-11000 CCD with 9x9 micron pixels and a full well capacity of 60,000 e⁻, both of these are mounted to a Paramount MX equatorial mount. Located in Oadby, Leicester (52.601°N, -1.081°W), the location proved to be unfortunately challenging due to the combination of trees surrounding the observatory providing a limited horizon, the weather consistently being overcast, providing few chances for observations, and although the light pollution in Oadby is relatively low at a Bortle Class 5 [11], the site was only about 100 meters away from a leisure centre which significantly increased light pollution in the surrounding area.

We observed three different exoplanet transits during our period of observation. However, an identical experimental setup was used for each observation, with the only exception being exposure times, which will be discussed in further detail in the Data Processing section 3.4. Therefore, during this section, the example of exoplanet XO-3 b will be discussed in detail, with the understanding that the same approach was used for the other two transit observations.

XO-3 b had a transit duration of 2.712 ± 0.136 hours [1], we observed the transit on March 5, 2025, assisted by the transit times provided by NASA's Transit Prediction Service [10]. The observation process began by setting up the telescope in the afternoon of the transit before sunset, this was to take flat field calibration photos. Flat field, dark and bias calibration photos will be discussed in further detail in a later section of the paper 3.4.

When the telescope and CCD had been turned on, we cooled the CCD sensor to 15°C cooler than ambient, and at this point, we needed to find the target exoplanet. As XO-3 b was not on SkyX[12] (software used to manage and control the telescope), we used co-ordinates provided by NASA's Transit Prediction Service [10] in conjunction with a finding chart to find and slew to XO-3 b. A finding chart is a map of a small region in the sky and can be used as a comparison image to our science frames to locate our target exoplanet. Finding charts used in this process were obtained from Astronomy at Swarthmore College's website [13], XO-3 b's finding chart is shown in 4.

Upon completion of data collection the telescope needed to be turned off, the process was mainly the reverse of the setting up with the exception being we had to ensure the CCD sensor warmed up without turning the fan off. This was to mitigate any condensation building up on the sensor as it was cooled to below ambient temperatures, the fan could then be turned off when the sensor was at ambient temperature. The computer used for the SkyX software was not to be turned off for the same reason.

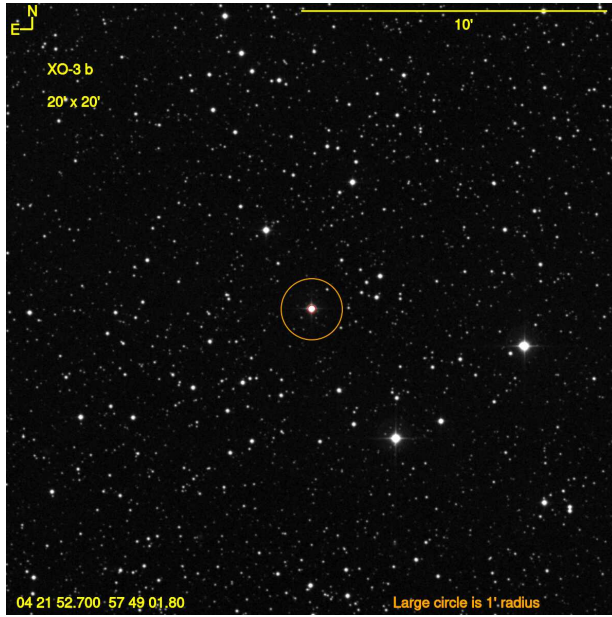


Figure 4: Example Finding Chart - XO-3 b. Source [13].

3.3 OBTAINING DATA

Before taking science frames, we took flat field calibration photos. This was done by pointing the telescope at an empty field of the sky as the sun was setting, ensuring it was still light enough to map out any dust, vignetting or optical imperfections, yet dark enough to not overexpose the sensor and cause clipping in the data. To achieve this brightness we took flat frames when peak counts were between 30,000 and 40,000. Counts, or number of photons

measure the brightness of an object in a frame and are discussed in detail in the Data Processing section 3.4. 15 Frames flat frames were taken with 1-second exposure times. After flat frames had been taken, and one hour before the ingress of the transit, we slewed the telescope to XO-3 b ready to take science frames. Setting up a sequence of 120 frames at 20-second exposures, to be repeated until an hour after the transit egress. Out-of-transit data was taken to obtain a baseline flux for the host star that can be used to normalize the flux during transit. Science frames were taken in the visible filter to capture as much light as possible. During observation, around every 30 minutes, we had to re-slew the telescope as the target had travelled across the frame of the image, this was unavoidable as the mount did not track the star perfectly as it travelled across the sky. However, it was not problematic and could be accounted for when analysing the data. The total duration of the observation was 160 minutes. A 20-second exposure was chosen for XO-3 b in order to keep the star at a high count rate, yet still below 60,000. Exposing the sensor for 20 seconds in this case kept the peak count rate for XO-3 at around 30,000.

After all the light frames had been taken, we took dark and bias calibration frames. Dark frames were taken by closing the shutter and turning off the lights, ensuring the CCD sensor was at the same temperature as when it took science frames, and then taking 10 frames at the same 20-second exposure as the science frames. Bias frames were taken in a similar manner except with a 0-second exposure time, 10 bias frames were taken.

3.4 DATA PROCESSING

Before the science images can be used for transit analysis, they need to be corrected and calibrated using the calibration frames taken whilst observing.

Calibration frames are taken to reduce the noise and remove sensor imperfections and artefacts. Improving the accuracy of the data. Flat field frames, or flats, are taken to ensure each pixel returns the same value for the same amount of exposed light, this can mitigate the effect of deformities in the sensor, dust mites, and vignetting. Other noises can be reduced by taking dark and bias calibration frames. Dark frames attempt to capture the thermal noise generated by the CCD sensor, this is something that we can minimize by ensuring the CCD is kept 20° cooler than ambient, usually around -15°C, however, it is not completely mitigated and dark frames are used to further remove thermal noise from science frames. The reason we could not cool the CCD further than 15° below ambient to further reduce thermal noise is to not overload the cooling system. Bias frames are used to calibrate the sensor's readout noise, average it out and remove it from the science frames. Example calibration frames can be seen in

appendix B.

To apply these calibrations to the science frames, we used the software *AstroImageJ*[3].

Firstly, the calibration frames needed to be combined into master calibration frames so that they could be applied to the science frames. This is done because each calibration frame contains a certain amount of random noise, and combining them reduces that noise, creating a cleaner and more effective calibration frame. This was done in *AstroImageJ*'s data reduction facility, inputting biases, flats and darks. The data reduction facility automatically combined the flats and darks using the bias frames to debias both. The combination method we used to create the master frames was the median method, this method finds the median pixel of each of the calibration frames and adds them to the master frame. This process is shown in appendix C.

Once master calibration frames had been made, they had to be applied to the science frames to remove noise and artefacts. This was also done automatically in the Data Reduction Facility by checking the box for 'Science Image Processing'.

At this point we had our calibrated science frames and needed to find comparison stars for the photometric analysis. Comparison stars are necessary for accurate and reliable brightness measurements of our host star, they capture atmospheric variability such as faint clouds travelling across the sky or brightness fluctuations in the environment. This variability can be subtracted from the brightness of the host star to ensure accurate measurements during analysis. For the best results, good comparison stars needed to be similar in brightness and colour to our target star, usually ranging from 5,000 to 20,000 counts, they also needed to be close to the target star to ensure any variability affects both the target and comparison star simultaneously.

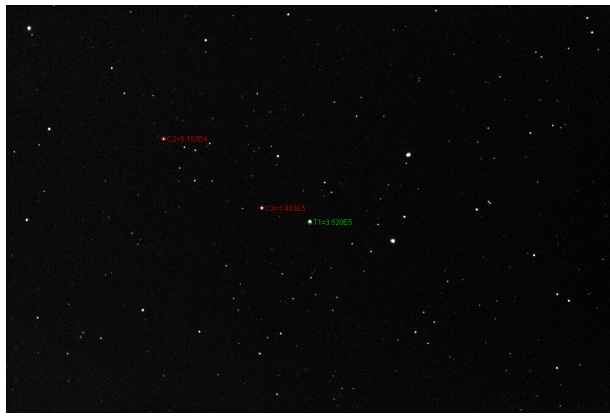


Figure 5: XO-3 b Science Frame with Comparison Stars [3].

Counts, or detected photons, can be measured in *AstroImageJ* using a seeing profile, which shows the counts on the

Gaussian curve of an object within a specific aperture. It is important to ensure that neither the comparison nor target star reach counts over 60,000, this is because the CCD at this point will become over-saturated. Over saturation occurs when a CCD pixel receives more light than its well can hold, causing electrons to spill into surrounding pixels, leaving an effect that is known as blooming on the resulting image, rendering it inaccurate and unusable. Figure 5 shows the target star XO-3 b as well as two comparison stars surrounding it, with the seeing profile for the target star XO-3 shown in figure 6. The two comparison star seeing profiles can be seen in appendix C. Seeing profiles are also useful for aperture size choice, displaying a half width half maximum (HWHM), source radius and background inner and outer radii. For the XO-3 b example, the source radius was six pixels and inner and outer background radii were 10 and 15 respectively, these were the aperture parameters used for the photometric analysis.

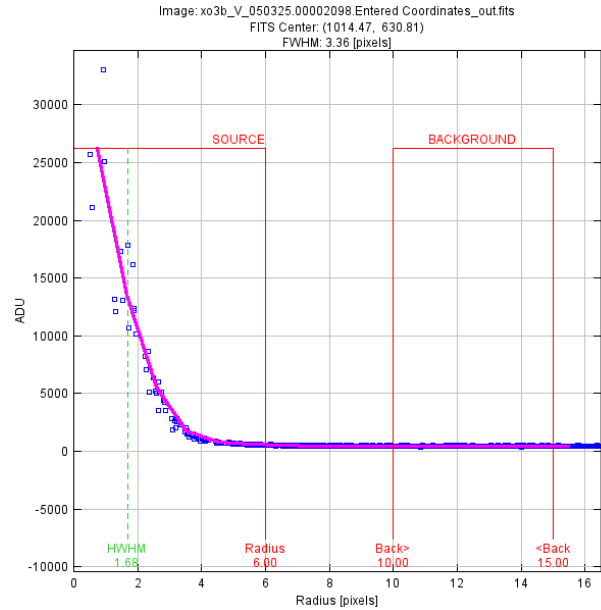


Figure 6: XO-3 b Seeing Profile [3].

Placing the apertures on the target and comparison stars we were able to begin photometric analysis, *AstroImageJ* would track the stars throughout the sequence of images however if the stars shifted (if the telescope had to be moved) too quickly the apertures had to be replaced and the process continued. Once the analysis was over, variables *rel.flux.T1* (relative flux) and *J.D.-2400000* (time), were plotted to create the light curve and areas out of transit are used to normalize the flux during transit. Data points were binned into bins of 12 and error bars were shown to help visualize the transit.

3.5 TRANSIT ANALYSIS

After plotting the points and creating our light curve, we had to fit a transit model to calculate the radius of the exoplanet. This was done by applying a transit fit mode in the plot settings, opening a new window called 'Data Set Fit Settings', where we could enter our planetary and stellar parameters, the algorithm used for transit model fitting by AstroImageJ is from Mandel & Agol (2002)[14]. Characteristics required were the exoplanet's orbital period and its host star's radius. A list of research papers including this information is given by NASA's exoplanet archive [9], we chose the most recent paper for the most up-to-date information on the exoplanet and its host star. AstroImageJ would automatically run this information through the transit model and calculate the exoplanet radius, plotting the predicted transit on the light curve. The transit model would also return statistical information on the transit model. Root mean Square Residuals (RMS Residuals) would calculate the average deviation from the observed data to the best-fit transit model, and the χ^2/DOF value assesses how well the model explains the observed data, the closer the χ^2/DOF to one the better the fit, with a value of one suggesting a perfect fit to the transit model.

Uncertainties for final radius values are calculated by inputting the upper and lower bounds of the stellar parameters used into the transit fit model. This is because the radius of the exoplanet is directly linked to the radius of the host star.

4 Results

A total of three transits were observed, each of a different exoplanet: HAT-P 61 b, XO-3 b and TOI-3887, with the final observation being of an unpublished candidate exoplanet. The first, HAT-P 61 b, was observed transiting its host star on February 24, 2025. From the Transit Prediction Service [10] ingress was at 18:41 and egress at 20:20. The host star, HAT-P 61, is a 13th magnitude G6 star [15], therefore an exposure of 60 seconds was required to collect sufficient light for analysis, with counts of the target star peaking around 4,600. Ideally, the target would be brighter between 10,000 - 20,000 counts but an exposure time too long would create streaks along the frame as the mount did not accurately track the star across the sky. A total of 130 science frames were taken totaling 130 minutes of exposure time. Only the egress of this transit was observed as the sky was not dark enough during the ingress of the transit, this can be seen in the airmass plot of the transit shown in figure 7.

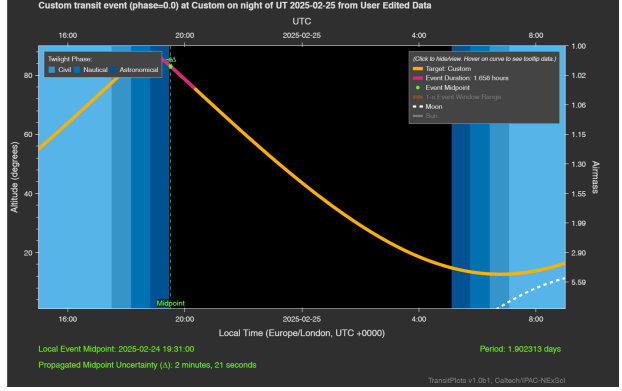


Figure 7: HAT-P 61 b Airmass Plot [10].

The light curve plotted can be seen in figure 8, with comparison stars plotted underneath to display atmospheric fluctuations throughout the observation.

Out of transit data is marked between the 'Right' and 'Right Trim' dotted lines. The transit is displayed as an orange line and had a transit depth of 0.764%, the transit model fit window for HAT-P 61 b along with the other two transits is shown in appendix D. With an orbital period of 1.9 days and host star mass of $1.004 \pm 0.033 M_{\odot}$ [4], the calculated exoplanet radius for HAT-P 61 b was $0.87 \pm 0.04 R_J$, with uncertainties being calculated from the upper and lower bounds of the stellar parameters used.

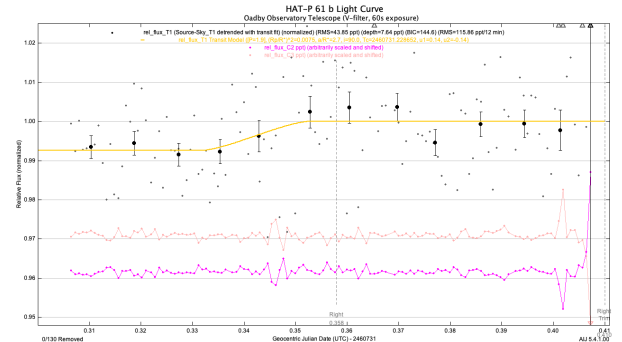


Figure 8: HAT-P 61 b Light Curve [3].

The second transit observed was of XO-3 b, an exoplanet orbiting the 10th magnitude F5V star XO-3 [15]. The observation took place on March 5, 2025. With an ingress at 19:19 and an egress at 22:02[10], we were able to observe the whole transit including out-of-transit data before ingress and after egress. Unfortunately during the transit, the moon was around 20° away from the target star increasing the background brightness and reducing the contrast between HAT-P 61 and the sky. The path of the moon and the target star can be seen in the airmass plot shown in figure 9. With XO-3 being a brighter star with an apparent magnitude of 10, we were able to measure more data points using a shorter exposure time of 20 seconds.

Taking 479 frames totaling 160 minutes of exposure time. Two comparison stars were chosen in close proximity and brightness to XO-3 and photometry data was plotted into a light curve shown in figure 10.

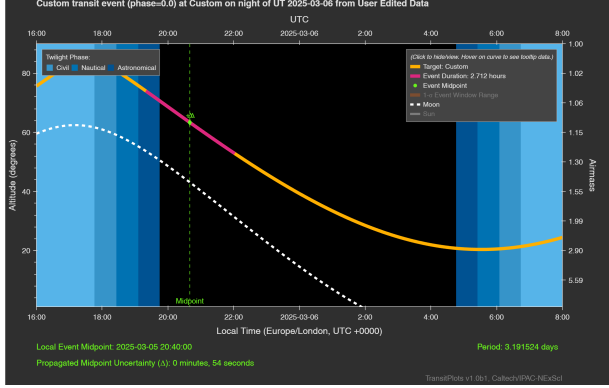


Figure 9: XO-3 b Airmass Plot [10].

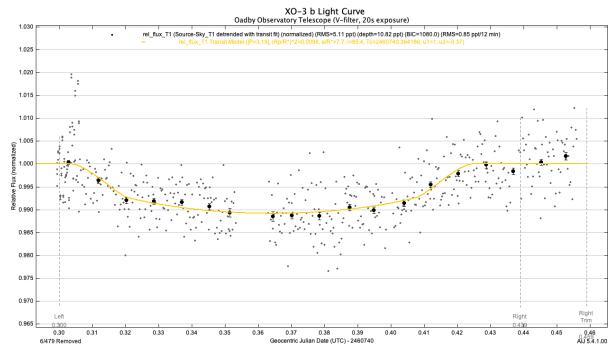


Figure 10: XO-3 b Light Curve [3].

The light curve shows a well-defined dip in measured flux from XO-3 with a measured transit depth of 1.082%. Using a stellar radius of $1.54 \pm 0.11 R_{\odot}$ and orbit period of 3.19 days [5], the transit model fit returned an exoplanet radius of $1.48 \pm 0.1 R_{J}$.

The final exoplanet observed was TOI-3887 on March 6, 2025, an unpublished candidate planet with exoplanet data from TESS [1] and stellar data from Gaia [2]. The host star was dim enough to once again require 60-second exposure times, a total of 285 science frames were taken totalling 285 minutes of exposure time. Comparison stars were chosen and the photometric data was plotted and can be seen in figure 11 below.

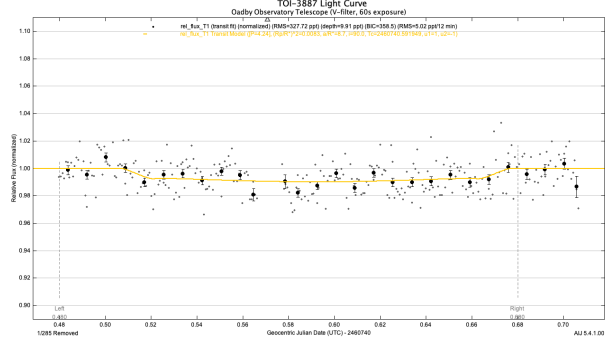


Figure 11: TOI-3887 Light Curve [3].

The dip in measured flux is not as well defined as the other two transits observed. This may have been due to worsening seeing conditions later in the night with the ingress being at 02:03 and egress at 04:02. Using an orbital period of 4.24424 days [1] and a stellar radius of $1.57 R_{\odot}$ [2], the calculated exoplanet radius for TOI-3887 was $1.39 R_J$ with a transit depth of 0.99%. Uncertainties have not been calculated for this radius as there have been no provided uncertainties in stellar radius, this is because they are a first-order estimate of stellar parameters fitted with stellar models from Gaia's collected data and are not confirmed parameters.

A table of calculated exoplanet radii along with relevant data is summarized in table 1.

5 Discussion

Comparing transit depth measurements, our literature used for HAT-P 61 b, Bakos et al. 2021 [4], does not conclude its own transit depth but uses light curves from ExoFOP-TESS TOI [1] with a transit depth of 1.07%. This is a transit depth 21.7% larger than our calculated value and is a large discrepancy considering final radius values are within 3.4%. This difference may be due to varying data analysis methods and the literature's involvement of spectroscopic data within the analysis.

Stassun et al. 2017[5], the chosen literature for comparison of XO-3 b's data, concluded a transit depth of $0.890 \pm 0.078\%$. A value 19.3% shallower than our measured depth of 1.08%, this is likely also due to different data analysis methods as well as the inclusion of impact parameters and orbital eccentricity.

The final exoplanet has no published data therefore we have no literature to compare our results with.

Calculated values of radii for HAT-P 61 b and XO-3 b both fall within one uncertainty bar of the chosen literary value. However, it is important to note that for each confirmed exoplanet there are several different studies each accompanying different methodologies and analysis techniques, each concluding different results. For exam-

Target	Orbital Period (days)	Host Star Radius (R_{\odot})	Transit Depth (%)	Calculated Radius (R_J)	Literary Radius (R_J)
HAT-P 61 b	1.9 ± 0.00000077	0.938 ± 0.011	0.76	0.87 ± 0.04	0.899 ± 0.027
XO-3 b	0.938 ± 0.011	1.54 ± 0.11	1.08	1.48 ± 0.1	1.41 ± 0.027
TOI 3887	4.244	1.57	0.99	1.39	Unconfirmed

Table 1: Exoplanet Transits Results.

ple, ExFOP-TESS TOI concludes a HAT-P 61 b radius of $1.015 \pm 0.067R_J$ [9], which is 2.125 uncertainty bars outside of our radius for the same planet. Knowing this, it is important to not definitively endorse any answer as correct or incorrect.

A main limitation of this project, briefly mentioned in section 3.2, was the weather and seeing conditions through the observational period, limiting the opportunities for transit observations to occur. If this project were to be repeated having more time to observe or observing during times of clear weather would have improved the reliability and accuracy of the results. More transit measurements, optimally repeat measurements for the same transit would have helped confirm the periodicity of the transits. As well as allowing for longer observation windows, gathering more out-of-transit data, ensuring we are able to compare transit timings and not mark incorrect ingress and egress times during analysis. The project was also limited to a single wavelength filter during measurements, this means that wavelength-dependent phenomena such as limb-darkening could not be accounted for during analysis. More measurements would have allowed for repeat measurements in different wavelength filters, allowing for limb-darkening modelling. Repeat observations of the same transit would have given rise to the opportunity for Transit Timing Variation (TTV) measurements, a technique that can reveal system complexity and other planetary bodies orbiting our target star.

Something that was briefly mentioned is the choice of target exoplanets, and that two of the three are not present on the transit candidate list. The reason for this links to the unfortunate weather and seeing conditions through the period of observation during the project. With very few clear nights and chances to use the Oadby observatory, when a chance to observe arose that did not have a planned transit on the candidate list, we would expand our search to include exoplanets with transits less than 0.8%. This would mean that the transit would be harder to measure with the telescope however we decided that a shallow transit is better than no observation at all. Transits observed that do not fit the filters described in section 3.1, have been added to the transit candidate list and have been highlighted to show that they were not in the original list.

Knowing the radius and orbital period of the target exo-

planets that we observed. It is possible to make estimates on the type of planets that they are and what they are made of. The estimations can be improved with the addition of mass data.

HAT-P 61 b, an exoplanet of radius $0.87 \pm 0.04R_J$ with an orbital period of 1.9 days, is likely to be a gas giant or a planet with a highly inflated atmosphere. The short orbital period indicates the planet is orbiting very close to its host star, and remains at a hot temperature, possibly leading to atmospheric evaporation. With this information, it is possible to conclude that HAT-P 61 b is likely a hot Jupiter. This idea is reinforced by the introduction of mass data. Bakos et al. 2021 [4] conclude a mass of $1.057 \pm 0.70M_J$ for HAT-P 61 b, aligning with the estimate that the exoplanet is a hot Jupiter as it gives a planetary density of 1.648 g/cm^3 , slightly higher than most hot Jupiters however that could just suggest factors such as an increased metallically or more compact structure.

The second exoplanet observed, XO-3 b, has a very short orbital period of 0.938 days, putting it in the category of an Ultra Short Period (USP) planet. USPs generally exhibit very high temperatures and experience large amounts of stellar radiation. This stellar radiation could be the cause of the large radius of the exoplanet, heating the planet and expanding the atmosphere. However, including mass data from Stassun et al. 2017 [5], XO-3 b is much more massive than most hot Jupiters at a mass of $7.29 \pm 1.19M_J$. Although at this size, it is unlikely that the planet is anything other than a gas giant and the high mass is likely suggesting of a more compact structure or a dense core made from heavier elements such as rock and metal.

The final planet that we observed was TOI-3887, an unpublished candidate exoplanet. It has an orbital period of 4.2442 days and we concluded its radius to be $1.39R_J$. At this orbital period, the exoplanet will still experience high temperatures and large amounts of stellar radiation, even if it is not at the same level as USP's. The radius is slightly larger than that of Jupiter, possibly suggesting an inflated atmosphere due to its close proximity to its host star. With this information, TOI-3887 is likely a warm or hot Jupiter. There is no published mass data to compare this estimation with.

Looking at the types of exoplanets observed, and that target exoplanets were chosen at random after applying

filters. Results may suggest that there is a bias toward larger gas giants when using the transit method. This is something that tends to be the case when using the transit method as it exhibits clear observational biases when being able to observe exoplanets.

The depth of the transit is one of the most fundamental variables when observing an exoplanet transit, and the deeper the transit depth the easier the planet is to detect via the transit method. Larger planets such as gas giants block out more light from their host stars and therefore create a deeper transit compared to smaller planets such as Earth-sized planets. Another factor affecting the transit depth is the orbital period, the closer an exoplanet orbits its host star, the more light it will block out. This suggests that the bias of the transit method is toward hot Jupiter-type exoplanets, which is consistent with our three target exoplanets.

As well as the depth of the transit, the frequency of transit plays a part in how likely an exoplanet is to be discovered via the transit method. Exoplanets with short orbital periods are likely to transit multiple times during missions like TESS and Kepler's observational window. Exoplanets orbiting further away from their host star may not transit at all even when being observed due to their long orbital periods.

However, even with the biases discussed the transit method displays, that this method is still the most suitable for the project. The second most successful method for detecting and confirming exoplanets is the radial velocity method, a method that relies on the periodic motion of a star caused by the gravitational pull by orbiting planets. The radial velocity method does not measure the size of the exoplanet but the mass, therefore incorporating both these methods within this project would not only further statistically confirm measured exoplanets but provide mass measurements that could be paired with the radius measurements to determine what types of exoplanets we are observing without the need for external data. Unfortunately, the radial velocity method requires high-resolution spectrometers which are expensive and have highly limited availability. Therefore it would be impractical to use both of these methods to gain information on these exoplanets, especially when observing for such a short period of time.

6 Conclusion

The purpose of this project was to target and observe an exoplanet's transit across its host star, calculating the exoplanet's radius from the analysis of the transit. This is something we completed for two different exoplanets and a candidate exoplanet, comparing our results to literary values, understanding that different literature conclude

varying results. Our first exoplanet, HAT-P 61 b measured a transit depth of 0.86%, which, using a stellar mass of $1.004 \pm 0.033 M_{\odot}$ [4], lead to a radius of $0.87 \pm 0.04 M_J$.

Our second exoplanet was XO-3 b, a transit depth of 1.08% was measured which gave an exoplanet radius of $1.48 \pm 0.1 M_J$, using a stellar radius of $1.54 \pm 0.11 R_{\odot}$ [5].

The third and final exoplanet observed was the unpublished candidate exoplanet TOI-3887, we measured a transit depth of 0.99%, and with a stellar radius of $1.57 R_{\odot}$ [2], led to an exoplanet radius of $1.39 M_J$.

Stellar parameters used in this project were obtained from previously published literature on each exoplanet where applicable, and radius uncertainty values were calculated directly from the incorporation of these stellar parameter uncertainties into the transit model. Uncertainties are not given for TOI-3887 as there are no associated uncertainties with the stellar radius used, this is because the data is still preliminary and does not have formal uncertainty calculations.

With the inclusion of mass data from each exoplanet's respective chosen literature, it was concluded that all three of the exoplanets observed are hot Jupiters orbiting close to their host star with a short orbital period.

If this project were to be repeated, improvements would likely arise from having more time to observe, or observing in a location with better seeing conditions. For example, the Very Large Telescope (VLT) in Chile, has a dry climate with low atmospheric turbulence and low light pollution. These are luxuries we did not have using the Oadby Observatory, therefore clear nights were rare and we were unable to pick and choose repeat transits, and when a chance to observe arose, seeing conditions were not optimal. Other improvements, a larger telescope mirror would have collected more light from the target star and allowed for shorter exposure times and more data points.

7 Statement of Personal Contribution

All of the data gathering during our time in the Oadby Observatory was done together as a group, apart from the TOI-3887 observation which was done by two members of the group. However, all of the data analysis was done individually after the observations.

References

- [1] Natalia M. Guerrero et al. “The TESS Objects of Interest Catalog from the TESS Prime Mission”. In: *The Astrophysical Journal Supplement Series* 254.2 (June 2021), p. 39. doi: [10.3847/1538-4365/abefe1](https://doi.org/10.3847/1538-4365/abefe1). URL: <https://iopscience.iop.org/article/10.3847/1538-4365/abefe1>.
- [2] Gaia Collaboration et al. “Gaia Data Release 3: Summary of the contents and survey properties”. In: *Astronomy & Astrophysics* 674 (2023), A1. doi: [10.1051/0004-6361/202243940](https://doi.org/10.1051/0004-6361/202243940). URL: <https://doi.org/10.1051/0004-6361/202243940>.
- [3] Karen A Collins et al. “ASTROIMAGEJ: IMAGE PROCESSING AND PHOTOMETRIC EXTRACTION FOR ULTRA-PRECISE ASTRONOMICAL LIGHT CURVES”. In: *The Astronomical Journal* 153.2 (Jan. 2017), pp. 77–77. doi: <https://doi.org/10.3847/1538-3881/153/2/77>. URL: <https://iopscience.iop.org/article/10.3847/1538-3881/153/2/77>.
- [4] G. Á. Bakos et al. “HAT-P-58b–HAT-P-64b: Seven Planets Transiting Bright Stars*”. In: *The Astronomical Journal* 162.1 (June 2021), p. 7. doi: [10.3847/1538-3881/abf637](https://doi.org/10.3847/1538-3881/abf637). URL: <https://iopscience.iop.org/article/10.3847/1538-3881/abf637>.
- [5] Keivan G. Stassun, Karen A. Collins, and B. Scott Gaudi. “Accurate Empirical Radii and Masses of Planets and Their Host Stars with Gaia Parallaxes”. In: *The Astronomical Journal* 153.3 (Mar. 2017), p. 136. doi: [10.3847/1538-3881/aa5df3](https://doi.org/10.3847/1538-3881/aa5df3). URL: <https://ui.adsabs.harvard.edu/abs/2017AJ....153..136S/abstract>.
- [6] Aleksander Wolszczan and Dale A. Frail. “A planetary system around the millisecond pulsar PSR1257 + 12”. In: *Nature* 355 (Jan. 1992), pp. 145–147. ISSN: 1476-4687. doi: [10.1038/355145a0](https://doi.org/10.1038/355145a0).
- [7] Jason W. Barnes. “Effects of Orbital Eccentricity on Extrasolar Planet Transit Detectability and Light Curves”. In: *Publications of the Astronomical Society of the Pacific* 119.859 (Sept. 2007), pp. 986–993. doi: <https://doi.org/10.1086/522039>. URL: <https://ui.adsabs.harvard.edu/abs/2007PASP..119..986B/abstract#:%text=The%20duration%20of%20a%20planet's,for%20a%20given%20impact%20parameter..>
- [8] W Hamme. “NEW LIMB-DARKENING COEFFICIENTS FOR MODELING BINARY STAR LIGHT CURVES”. In: 106.5 (1993). URL: <https://ui.adsabs.harvard.edu/abs/1993AJ....106.2096V/abstract>.
- [9] NASA Exoplanet Science Institute. *NASA Exoplanet Archive*. Accessed: Feb-2025. 2025. URL: <https://exoplanetarchive.ipac.caltech.edu>.
- [10] NASA Exoplanet Archive. *Transit Prediction Service*. Accessed: Feb-2025. 2025. URL: <https://exoplanetarchive.ipac.caltech.edu/cgi-bin/TransitView/nph-visibletbls>.
- [11] Light Pollution Map. *Light Pollution Map*. Accessed: Feb-2025. 2015. URL: <https://www.lightpollutionmap.info>.
- [12] Software Bisque. *TheSkyX Astronomy Software*. 2024. URL: <https://www.bisque.com>.
- [13] Swarthmore College Astronomy Department. *Transit Finding Charts*. Accessed: Feb-2025. 2025. URL: https://astro.swarthmore.edu/transits/finding_charts.cgi.
- [14] K. Mandel and E. Agol. “Analytic Light Curves for Planetary Transit Searches”. In: *The Astrophysical Journal Letters* 580.2 (2002), pp. L171–L175. doi: [10.1086/344704](https://doi.org/10.1086/344704).
- [15] Exoplanet Kyoto Team. *Exoplanet Kyoto Database*. Accessed: 2025-03-16. 2019. URL: <https://www.exoplanetkyoto.org/?lang=en>.

A Transit Candidate List

Planet Name	Transit Ingress	Transit Egress	Acceptable	Notes
K2-30 b	31/01/2025 19:17	31/01/2025 21:36	Y	Perfect
XO-3 b	01/02/2025 21:21	02/02/2025 00:04	Y	Perfect
WASP-104 b	02/02/2025 02:07	02/02/2025 03:54	Y	late
HAT-P-30 b	02/02/2025 22:24	03/02/2025 00:39	Y	Perfect
WASP-12 b	03/02/2025 20:54	03/02/2025 23:57	Y	Perfect
WASP-56 b	06/02/2025 00:42	06/02/2025 04:15	Y	late
TOI-2154 b	06/02/2025 02:22	06/02/2025 04:53	Y	Perfect, late at night
XO-2 N b	07/02/2025 00:08	07/02/2025 02:39	Y	Perfect, late at night
HAT-P-12 b	07/02/2025 00:45	07/02/2025 02:55	Y	late
Qatar-8 b	07/02/2025 22:22	08/02/2025 02:12	Y	
HAT-P-22 b	08/02/2025 21:29	09/02/2025 00:08	Y	
TOI-1811 b	09/02/2025 00:40	09/02/2025 02:19	Y	
KELT-3 b	10/02/2025 00:06	10/02/2025 03:01	Y	
HAT-P-39 b	12/02/2025 21:16	13/02/2025 01:30	Y	might be low but is fine
HAT-P-20 b	12/02/2025 21:25	12/02/2025 23:02	Y	Perfect
XO-2 N b	14/02/2025 20:28	14/02/2025 22:59	Y	Perfect
WASP-12 b	15/02/2025 21:03	16/02/2025 00:06	Y	Perfect
XO-3 b	17/02/2025 20:20	17/02/2025 23:03	Y	Perfect
KELT-4 A b	18/02/2025 21:47	19/02/2025 01:08	Y	
KELT-3 b	20/02/2025 19:37	20/02/2025 22:33	Y	
KELT-4 A b	21/02/2025 21:32	22/02/2025 00:53	Y	
KELT-4 A b	24/02/2025 21:17	25/02/2025 00:38	Y	
HAT-P-22 b	24/02/2025 22:57	25/02/2025 01:36	Y	
HAT-P 61 b	24/02/2025 18:41	24/02/2025 20:20	Y	New Entry
HAT-P-3 b	25/02/2025 00:49	25/02/2025 02:40	Y	late
HAT-P-36 b	26/02/2025 00:02	26/02/2025 02:07	Y	late
WASP-12 b	27/02/2025 21:11	28/02/2025 00:14	Y	May be low, not sure
XO-2 N b	27/02/2025 22:23	28/02/2025 00:54	Y	Perfect
HAT-P-3 b	27/02/2025 22:24	28/02/2025 00:15	Y	
KELT-3 b	28/02/2025 22:16	01/03/2025 01:12	Y	
HAT-P-36 b	01/03/2025 23:36	02/03/2025 01:41	Y	
WASP-104 b	03/03/2025 22:20	04/03/2025 00:06	Y	
TOI-2154 b	04/03/2025 20:49	04/03/2025 23:20	Y	Perfect
XO-3 b	05/03/2025 19:19	05/03/2025 22:05	Y	New Entry
HAT-P-30 b	05/03/2025 20:24	05/03/2025 22:39	Y	Perfect
WASP-65 b	05/03/2025 21:45	06/03/2025 00:29	Y	Perfect
Qatar-8 b	05/03/2025 22:25	06/03/2025 02:15	Y	
HAT-P-36 b	05/03/2025 23:10	06/03/2025 01:15	Y	
TOI-3887	06/03/2025 02:03	06/03/2025 04:02	Y	New Entry
HAT-P-9 b	06/03/2025 21:53	07/03/2025 01:05	Y	Perfect
TOI-1811 b	07/03/2025 00:28	07/03/2025 02:07	Y	
HAT-P-12 b	07/03/2025 22:46	08/03/2025 00:57	Y	
KELT-4 A b	08/03/2025 20:16	08/03/2025 23:37	Y	
HAT-P-36 b	09/03/2025 22:44	10/03/2025 00:49	Y	
HAT-P-9 b	10/03/2025 20:01	10/03/2025 23:14	Y	Close to moon at egress
WASP-65 b	12/03/2025 20:10	12/03/2025 22:55	Y	Close to moon
WASP-56 b	14/03/2025 23:10	15/03/2025 02:44	Y	

Table 2: Transit Candidate List.

B Calibration Frames

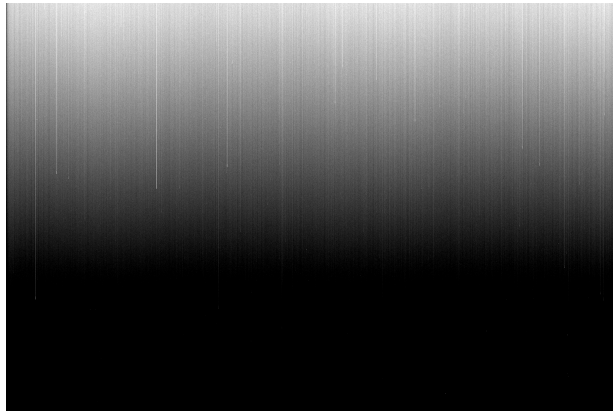


Figure 12: Master Bias Calibration Frame [3].

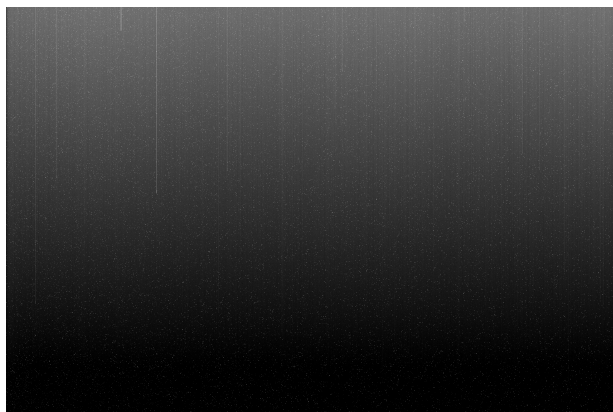


Figure 13: Master Dark Calibration Frame [3].

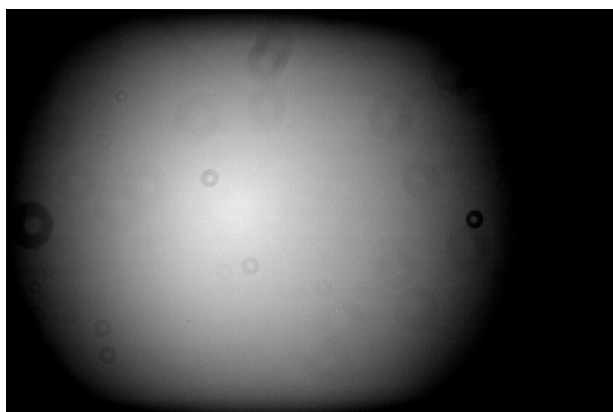


Figure 14: Master Flat Calibration Frame [3].

C Data Processing

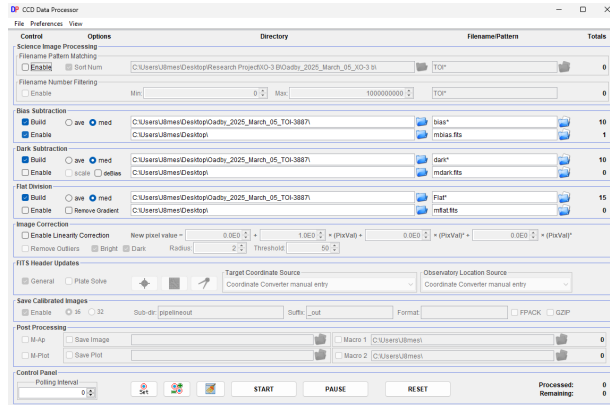


Figure 15: AstroImageJ Data Reduction Facility [3].

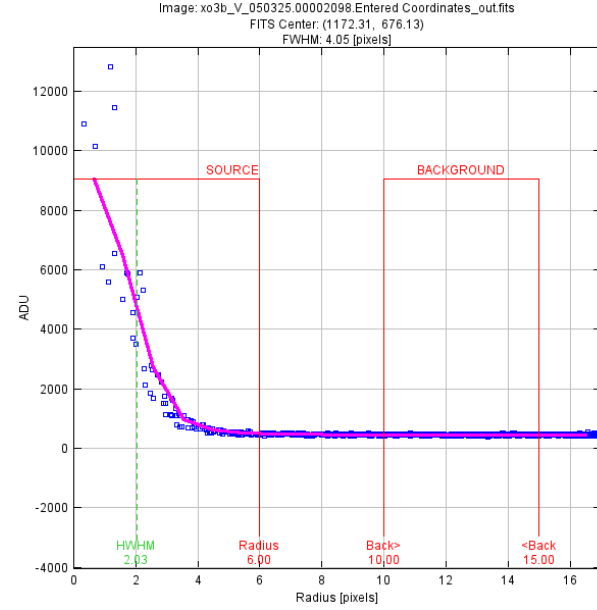


Figure 17: Comparison Star 2 Seeing Profile [3].

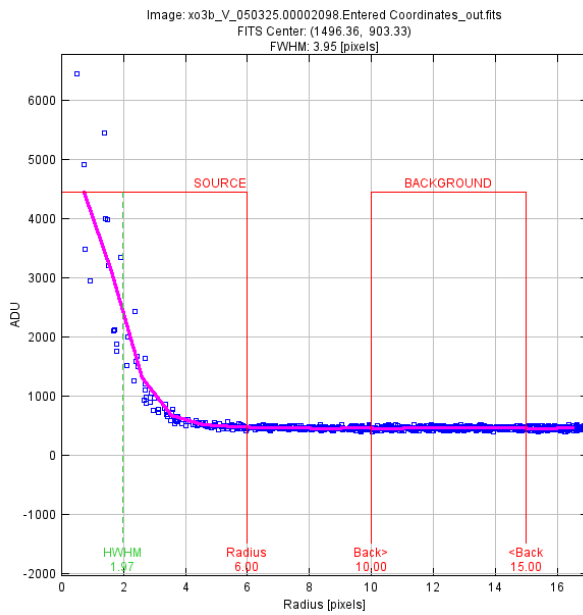


Figure 16: Comparison Star 1 Seeing Profile [3].

D Results



Figure 18: Transit Model Fit for HAT-61 b [3].

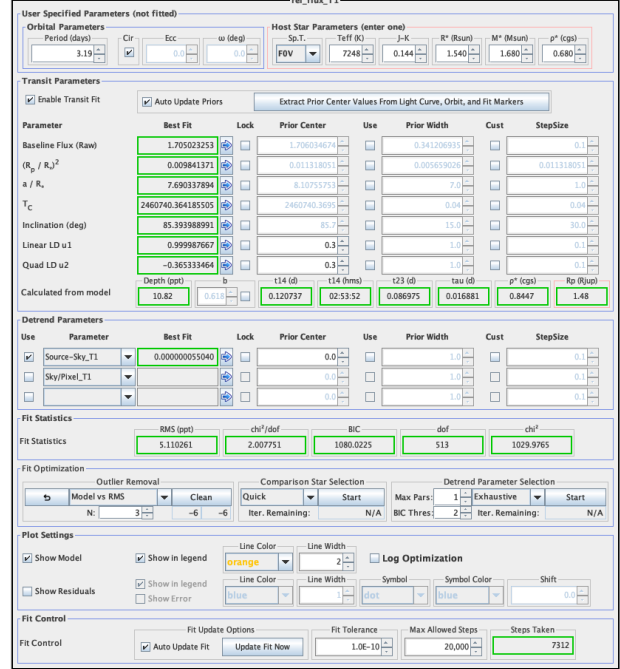


Figure 19: Transit Model Fit for XO-3 b [3].

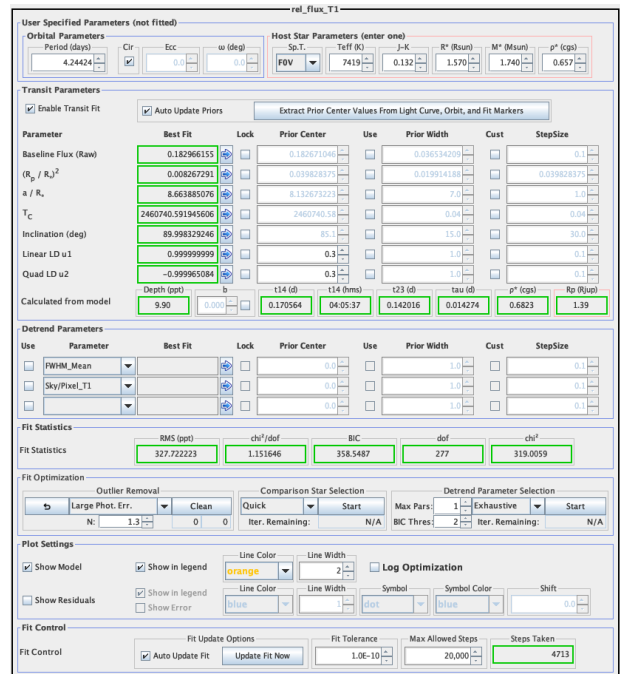


Figure 20: Transit Model Fit for TOI-3887 [3].